TU Delft

Delft University of Technology

# A blended continuum damage and fracture mechanics method for progressive damage analysis of composite structures using XFEM

van Dongen, Björn; van Oostrum, Alexander; Zarouchas, Dimitrios

**DOI**
10.1016/j.compstruct.2017.10.007

**Publication date**
2018

**Document Version**
Accepted author manuscript

**Published in**
Composite Structures

**Citation (APA)**
van Dongen, B., van Oostrum, A., & Zarouchas, D. (2018). A blended continuum damage and fracture mechanics method for progressive damage analysis of composite structures using XFEM. *Composite Structures*, *184*, 512-522. https://doi.org/10.1016/j.compstruct.2017.10.007

**Important note**
To cite this publication, please use the final published version (if applicable).
Please check the document version above.

**Copyright**
Other than for strictly personal use, it is not permitted to download, forward or distribute the text or part of it, without the consent of the author(s) and/or copyright holder(s), unless the work is under an open content license such as Creative Commons.

**Takedown policy**
Please contact us and provide details if you believe this document breaches copyrights.
We will remove access to the work immediately and investigate your claim.

*This work is downloaded from Delft University of Technology.*
*For technical reasons the number of authors shown on this cover page is limited to a maximum of 10.*

# A blended continuum damage and fracture mechanics method for progressive damage analysis of composite structures using XFEM

Björn van Dongen[1], Alexander van Oostrum[1], Dimitrios Zarouchas[1,*]

*Faculty of Aerospace Engineering, Delft University of Technology, Kluyverweg 1, Delft*

**Abstract**

Progressive damage analysis of composite structures remains problematic, holding back the full potential of these materials. Widely used continuum damage models feature a heuristical stiffness reduction to reflect damage, resulting in an unrealistic representation of damage patterns. To the end of a more realistic failure representation, this paper proposes a blended methodology for progressive damage analysis of such structures implemented in ABAQUS, combining continuum damage models with a more physically based approach from a fracture mechanics perspective. Matrix cracks are modelled through the eXtended Finite Element Method and delaminations through a cohesive zone model. Validation of the blend on an experimental campaign of open-hole tensile tests shows remarkable predictive capability, in good conformance to experimental failure loads, digital image correlation and acoustic emission measurements - particularly yielding more realistic damage patterns than state-of-the-art continuum damage model implementations.

*Keywords:* Composites, Finite Element Analysis, Damage mechanics, XFEM, cohesive zone modeling

*Corresponding author

*Email address:* d.zarouchas@tudelft.nl (Dimitrios Zarouchas)

## 1. Introduction

Propelled by advantages in structural efficiency, performance, versatility and cost, fibre-Reinforced Polymers (FRPs) have made a mark in numerous industries, aerospace industry being a leading party. The full potential offered by FRPs is held back, however, by an overall lack of understanding and inability to accurately predict failure [1, 2]. Composite anisotropy and heterogeneity complicate mechanical behaviour. These complications are particularly pronounced in Progressive Damage Analysis (PDA), exemplified by The World-Wide Failure Exercises [2, 3] reflecting an overall lack of prediction accuracy amongst leading failure theories.

Driven by the need for accurate failure prediction, great strides have been made in the development and implementation of failure theories for FRPs. These strides have mostly focused on isolated application of Continuum Damage Models (CDMs) on one hand and fracture mechanics on the other hand. CDMs, operating on the principle of damage initiation on the basis of the local stress-strain state [4, 5] and subsequent stiffness degradation to reflect damage [6], have found widespread application. Fracture mechanics approaches have been used most widely in the modelling of delaminations and to a limited extent matrix cracking. Fracture mechanics based approaches typically employ either the Virtual Crack Closure Technique (VCCT) or Cohesive Zone Models (CZMs).

Contrary to many of these past attempts, focusing on isolated application of these approaches, this paper presents a blended model combining both approaches for Progressive Damage Analysis (PDA) of FRPs. To this end, the paper commences with an abridged overview of CDMs and fracture mechanics approaches to PDA of FRPs. This is followed upon by the numerical implementation in ABAQUS. Thereafter, validation is presented with respect to an experimental campaign. Lastly, conclusions and recommendations are given.

## 2. Continuum Damage Models

CDMs operate on the basis of damage initiation criteria evaluating the local stress-strain state [4, 5], and propagation models, or Material Degradation Models (MDMs), that degrade material stiffnesses upon damage initiation [6]. Common to CDMs is a lacking strong physical basis, instead posed more on a heuristical basis - in particular for MDMs. Still, remarkable advancements have been made leading to the failure theories discussed briefly hereafter.

For the case at hand, the LaRC05 criteria are used to guide damage initiation from a stress and strain based methodology, complemented by the bilinear softening law formulated by Lapczyk and Hurtado [7] and extended to three dimensions by Zhang et al. [8] . This selection follows from a precursor study [9], to which the reader is referred for more details.

### *2.1. Initiation criteria*

Initiation criteria find their origin in the Tsai-Hill failure criterion [10, 11], proposed on the basis of the Von Mises yield criterion extended to anisotropic metals [12]. A fundamental flaw herein is overlooking composite heterogeneity, transferring to many mode-independent criteria in its wake (e.g. Hoffman [13], Chamis [14], Tsai and Wu [11] and Sandhu [15] criteria).

This deficiency instigated the development of mode-dependent criteria for a more correct assessment of the various intralaminar damage modes in FRPs, distinguishing tensile and compressive matrix and fibre failure [4, 5, 1]. Hashin and Rotem were the first to make this distinction to pose a set of criteria based on logical reasoning [16], followed upon by the more physically based Hashin criteria [17].

This led to the development of state-of-the-art failure theories. A key contribution and leading theory was posed by Puck and Schürmann [18, 19]. A

strong physical foundation, extending from the Mohr-Coulomb fracture theory for brittle materials, lends strength to its predictions. Past implementations have found good agreement with experimental results [2, 3]. In its wake, LaRC criteria were formulated on a similar basis, but extending in particular the treatment of fibre kinking [20, 21, 22]. The latest installment, the LaRC05 criteria, is at the forefront in terms of physically based intralaminar damage initiation criteria. A different, more empirical approach was taken by Cuntze and Freund, describing damage on the basis of the Failure Mode Concept [23, 24], yielding predictive accuracy on par with Puck and LaRC05 criteria [2, 3].

### *2.2. Material Degradation Models*

Stiffness reduction in the constitutive relationship by means of a MDM reflects the effect of damage in CDMs [6, 25]. Reduction can be either instantaneously or gradually. Traditionally, sudden MDMs have been used, showing little physical basis, but offering a simple and effective approach for PDA [26, 27, 28, 29].

Gradual MDMs are arguably better able to capture the physical nature of the damage process. A prominent form of gradual degradation is the bilinear softening law, guiding the degradation by means of fracture energies [30, 31, 7, 8]. In conjunction with the Matzenmiller et al. damage matrix [32], these bilinear softening models have yielded good accuracy [33, 34, 30, 31, 7, 8]. These softening laws offer the additional benefit of alleviating mesh dependence through the crack band model of Bažant and Oh [35] and alleviating convergence issues in implicit schemes through gradual stiffness reduction.

## 3. Fracture mechanics

Fracture mechanics models typically employ either VCCT or CZMs. VCCT has a relatively strong physical basic in the framework of LEFM and has found extensive use for cases in which the crack path is known in advance [36, 37].

Their use in composites is most widespread for the modelling of delaminations in which interface nodes are released to model the progression of cracks. Some authors, however, consider the sharp crack tips assumed in LEFM unphysical for damage in composites, such as delaminations, and rather argue that failure occurs over a process zone [38, 39]. CZMs employ this principle using traction-separation laws which define a gradual softening behaviour over the interface [38]. For the model presented in this paper a CZM is used for modelling both the delaminations and matrix cracks (in conjunction with XFEM), in light of the following advantages of CZMs:

1. No precrack is required as opposed to VCCT, making CZM very suitable for a general framework;
2. Progression of damage is embedded in their formulation and requires no mesh updating;
3. Multiple cracks are allowed to join without any special formulation.

A number of disadvantages apply to CZMs:

1. No distinction between shear modes (mode II & III) as no crack front is explicitly modelled [40];
2. Very fine meshes are required [41, 42];
3. A lacking strong physical foundation [37]. Recent experimental evidence suggests that interfacial damage is not confined to the interface and the interfaces follow a trapezoidal traction-separation law [43], contrary to what CZMs assume [44, 45, 42, 46].

## 4. Blending and numerical implementation

Numerical implementation is performed in ABAQUS [47], extended with user subroutines for material constitutive behaviour and CDM implementation (UMAT) and damage initiation for XFEM (UDMGINI). These components are individually discussed hereafter, followed upon by a discussion on blending and model integration.

### *4.1. UMAT*

Material constitutive behaviour and damage initiation and propagation for the CDM are defined in a UMAT, called at each integration point. At each increment, the local variables are passed onto the UMAT. In the UMAT, the following actions take place subsequently:

1. The local stresses and strains are retrieved and subsequently used to evaluate failure criteria. Material properties required are read in from an external input file, containing a library of materials.
2. When damage is detected, damage variables are updated and - if viscous regularization is adopted - gradually increased.
3. The damage variables act as flags to indicate whether property degradation is to take place. Property degradation follows as a direct reduction in material stiffness parameters, passed into the Jacobian.
4. The updated (damaged) stiffness matrix or Jacobian is used to update the stress tensor after incrementing the strain. The updated stress and strain tensor form the basis for the following iteration, passed into the main routine along with the defined Jacobian.

Damage initiation is designated by LaRC05 criteria for tensile and compressive fibre and matrix damage [21]. Stiffness degradation is performed through the three-dimensional bilinear softening model as implemented by Zhang et al. [7, 8].

### *4.2. Cohesive zones*

Cohesive zones for delaminations are implemented using ABAQUS integrated COH3D8 elements. An intrinsic formulation is used in which these elements are inserted between all plies except for those at the symmetry interface. An initial stiffness is provided using 50 times the out of plane ply stiffness. Damage is defined using quadratic failure criterion and the softening behaviour is given by a linear softening law. Mixed-mode behaviour is incorporated by using the Benzeggagh-Kenane interaction law [48]. Artificial viscosity

is adopted for cohesive zones to improve the rate of convergence [7, 33]. The viscosity parameter was based on a convergence study, yielding a value of $1 \cdot 10^{-5}$. This parameter is ideally kept small to minimize the artificial increase in energy associated with the introduction of this parameter.

To alleviate mesh dependence and reduce computational efforts typically associated with cohesive zones, interface strengths were reduced following the methodology by Turon et al. [42] based on the local element size. Reduction factors were similar for mode I and mode II, and of the order 2.0-2.5. Reported strengths are uncorrected.

### *4.3. Matrix cracking*

Matrix cracks in the plies are modelled using XFEM and cohesive zones. Local enrichment takes place using XFEM and phantom nodes allow mesh-independent fracture at these locations [49, 41, 31]. A user subroutine UDMGINI defines damage initiation following the Puck criteria [50]. Cracks are progressed if subsequent elements satisfy the same damage initiation criteria. Created fracture surfaces are connected using cohesive zones to model the separation behaviour. Fracture angles in plies are limited to planes parallel to the local fibre orientation, as per experimental evidence [31, 51, 52, 41]. Enrichments is used on a ply-to-ply basis using the cohesive interfaces for delaminations as a natural separation. Fracture toughness of inserted cohesive segments are taken the same as for delaminations [53].

The use of Abaqus for XFEM has its limitations. Most predominantly, in this paper, only one crack can be captured per side, per ply. Without the use of advanced selection of enrichment regions (outside the scope of this paper) this can not be circumvented. As a consequence thereof, there is a risk of underestimating the extent of damage due to the inability to capture additional, secondary matrix cracks.

Moreover, cracks grow from element edge to element edge in discrete steps and cannot feature a crack tip singularity. Although singularities for matrix cracks are of a lower order [54] than assumed in classical LEFM, this is still a

notable shortcoming.

### *4.4. Model integration*

Model components are integrated to yield three models as depicted in Figure 1. DM1 and DM2 denote the CDM using LaRC05 initiation and bilinear softening in the UMAT, without and with cohesive interface elements for delamination modelling respectively. DM3 denotes the fully blended model, where matrix cracks are modelled using cohesive zones inserted by XFEM (through the UDMGINI subroutine) and delaminations using cohesive interface elements, and the constitutive behaviour and fibre failure are modelled in the UMAT. Three models are evaluated, in order to assess the merits of CDM, those of cohesive zones for intralaminar failure and those of the discrete crack model.

[FLOWCHART INTEGRATION (Figure 1 APPROXIMATELY HERE]

## 5. Validation with experimental campaign

Experimental campaigning has been performed, in the form of open-hole tensile testing on Carbon-fibre Reinforced Polymer (CFRP) specimens, in order to validate and compare the developed methodologies. This model assessment focuses on the predictive capability of methods, in terms of final failure predictions, local damage patterns, damage evolution and strain field representation.

This section commences with a description of the experimental campaign, proceeds with a brief paragraph on the numerical modelling thereof, and concludes with extensive comparison of predictions to experimental results.

### *5.1. Experimental campaign*

Five specimens were manufactured from AS4/8552 unidirectional prepreg plies of 0.17 mm nominal thickness. Laminates were autoclave cured according to the cure cycle recommended by Hexcel [55]. Specimens contain 16 plies in a $[45^\circ\ /\ -45^\circ\ /\ 0^\circ\ /\ 90^\circ]_{2s}$ lay-up, with length 250 mm, width 25 mm and a hole diameter of 6.35 mm. Specimens were cut to size using a diamond cutting

blade and holes were drilled using carbide drill bits.

Quasi-static testing was performed on a 60 kN MTS test bench, see Figure 2, at a displacement rate of 1 mm/min. In order to assess the specimen state during loading, multiple inspection techniques have been employed:

- Three-dimensional Digital Image Correlation (DIC) to acquire full-field deformation mapping, using a Vic-3D Digital Image Correlation Measurement System. A black-and-white speckle pattern was painted on specimens to improve correlation quality. The set-up is shown in Figure 2a, consisting of dual camera's mounted and calibrated for a full-field image of the specimen near the hole.

- Acoustic Emission (AE) to determine the number and severity of damage events during loading through amplified acoustic signals [56]. Two VS900-M piezoelectric sensors were placed on each specimen, greased for good attachment and conduction, see Figure 2b. Sensors were placed asymmetrically for the purpose of damage localization. Sensor signals were preamplified using a 34 dB preamplifier, the threshold was selected 60 dB and the AE signals were processed using a Vallen AMSY-6 instrument.

[FIGURE SETUP EXPERIMENTAL (Figure 2) APPROXIMATELY HERE]

The typical failure pattern is as depicted in Figure 3. All specimens exhibit exclusively this damage pattern, characterized by:

- Pull-out type failure. fibre breakage at the ultimate load with extensive matrix cracking.

- Significant matrix cracking along the fibres, from the hole edge spanning the width of the specimen. In particular, extensive matrix cracking can be observed in the outer $\pm 45^\circ$ plies.

- fibre fracture in the $0^\circ$ plies, from the hole edge spanning the width of the specimen, effecting a full separation of these plies.

- Delaminations, from the hole edge spanning the width of the specimen, in most of the layers.

These patterns are visible in more detail through X-ray Computed Tomography (CT) scans, shown in Figure 4. Scans were performed after ultimate failure in order to provide a volumetric image of the visual state of damage.

[FIGURE FAILURE PATTERN (Figure 3) APPROXIMATELY HERE]

[FIGURE FAILURE PATTERN CT (Figure 4) APPROXIMATELY HERE]

Final failure loads obtained for the six specimens tested up to failure are given in Table 1, including the Coefficient of Variation (CV). Results show limited scatter, around an average of 26.2 kN.

[TABLE FINAL FAILURE EXPERIMENTAL (Table 1) APPROXIMATELY HERE]

### *5.2. Numerical modelling*

A $[45°, -45°, 0°, 90°]_{2s}$ lay-up is modelled as eight layers of C3D8 elements, one per ply, with cohesive zones interspersed. Symmetry is only used in through-thickness direction in view of laminate symmetry. The laminate is clamped at one end, and a uniform axial displacement is applied at the other end.

Material properties and model-specific parameters are given in Table 3, along with the cohesive parameters. In-situ parameters were estimated using the model proposed by Camanho et al. [57] to reflect the effect of ply embeddedness and thickness on apparent resistance to fracture (as first observed by Parvizi et al. [58]). Orthotropic thermal expansion is assumed, with $\alpha_1 = 0.0$ $°C^{-1}$ and $\alpha_2 = 3.0 \cdot 10^{-5}$ $°C^{-1}$ [59] and $\Delta T = 160°C$ [55].

[TABLE MATERIAL PROPERTIES (Table 3) APPROXIMATELY HERE]

### *5.3. Results and discussion*

Model predictions are compared to experimental observations, in terms of final failure loads, DIC observations and AE measurements. Moreover, damage patterns are evaluated - primarily to highlight the shortcomings of CDMs.

#### *5.3.1. Final failure loads*

Final failure loads are compared to the experimental failure load in Table 1. All models achieve good correspondence to the average experimental faillure load of 26.2 kN, corresponding to a failure stress of 385 MPa, errors to within 5 %. DM2 achieves slightly poorer correspondence, attributed to a discrepancy in failure patterns particularly in terms of delaminations. These results conform to results obtained earlier for CDMs, namely that in the absence of severe delaminations these are capable of delivering good global predictions [9]

[TABLE FINAL FAILURE LOADS (Table 1 APPROXIMATELY HERE]

#### *5.3.2. Damage patterns*

Damage patterns are given in Figures 5-6 in terms of matrix failure, and in Figures 7-10 in terms of delaminations, at 90 % of the predicted failure load. Critical failure is due to fibre failure in the $0^\circ$ plies, predicted similarly by all models, see Figure 11.

Extensive matrix cracking is observed in $\pm 45^\circ$ and $90^\circ$ plies. Matrix cracking in the $-45^\circ$ ply is depicted in Figure 5. The CDM of DM1 and DM2 shows a large amount of damage smearing, strongly contrasting with the discrete crack predicted by DM3. In particular, the CDM fails to respect fibre-matrix heterogeneity that causes matrix cracks to grow along the fibres. This key flaw associated with CDMs was shown previously to contrast strongly with experimental observations [9, 31, 52, 51].

Similar behaviour can be observed in the $90^\circ$ plies, see Figure 6. $0^\circ$ plies show little damage, while $45^\circ$ plies show a damaged state highly similar to that in the $-45^\circ$ plies.

These observations conform to observations made post-failure, see Figure 4. Moreover, the observed damage patterns show that the aforementioned limitation of single crack modelling does not impede accuracy significantly for the case at hand. Cracks are namely concentrated in a single band for all layers, although the $-45^\circ$ ply shows noticeable secondary cracking.

Still, however, this relates only to visible cracking for the case at hand. There are possibly more, unopened, secondary cracks that the model fails to capture. Moreover, for different loading configurations and specimens, this limitation may be significantly more pronounced.

Delamination predictions are given in Figures 7-10. Delaminations are predicted significantly more extensively for DM2 than for DM3. Underlying cause may be poorly modelled matrix crack-delamination interaction, as mentioned by Van der Meer [31]. Regrettably, experimental quantification of delaminations could not be performed. Therefore, the accuracy of delamination modelling cannot be precisely quantified.

[FIGURE DAMAGE MATRIX FAILURE - 45 (Figure 5) APPROXIMATELY HERE]

[FIGURE DAMAGE MATRIX FAILURE - 90 (Figure 6) APPROXIMATELY HERE]

[FIGURE DAMAGE DELAMINATION 45/-45 (Figure 7) APPROXIMATELY HERE]

[FIGURE DAMAGE DELAMINATION -45/0 (Figure 8) APPROXIMATELY HERE]

[FIGURE DAMAGE DELAMINATION 0/90 (Figure 9) APPROXIMATELY HERE]

[FIGURE DAMAGE DELAMINATION 90/45 (Figure 10) APPROXIMATELY HERE]

[FIGURE DAMAGE fibre FAILURE 0 (Figure 11) APPROXIMATELY HERE]

*5.3.3. Strain field representation*

Experimental observations are compared to model predictions in terms of strain maps at 10 % and 95 % of the experimental failure load in Figure 12 and 13 respectively. The spectrum is based on limits of DIC observations, in order to provide a high-contrast image where discrepancies are clearly visible in model predictions as white regions. At 10 % of the failure load, all models are in close correspondence to DIC observations, validating the constitutive model implemented in the UMAT subroutine.

For increasing severity of damage, culminating in the damaged state at 95 % of the failure load, agreement becomes noticeably poorer for DM1 and DM2. DIC observations dispute the heuristic stiffness reduction featured in these models, instead showing little if any effect of damage on the strain map in the outer ply. This conforms much more closely to the blended model, merely showing a local increase in strain around the developing matrix crack in 45°direction.

[FIGURE DIC 10 % (Figure 12) APPROXIMATELY HERE]

[FIGURE DIC 95 % (Figure 13) APPROXIMATELY HERE]

*5.3.4. Damage evolution*

Predictions can be compared qualitatively to AE observations, offering an on-line assessment of the rapidity and severity of damage evolution. Quantitative comparison is substantially more difficult, due to the noise received by AE and the additional requirement of a translation of element damage to energy release. This energy release is representative of the number of damage events, detected as incoming signals above a 60 dB threshold.

The measured energy is depicted in Figure 14a, compared to model predictions in Figures 14b-14d. The latter show the percentage of damaged elements per damage mode. These are normalized, in order to highlight the rapidity of the damage growth (rather than the extent of damage), resulting in the damage patterns discussed previously.

Figure 14a shows that energy release starts at roughly 40 % of the failure load, developing initially at a relatively slow pace but at an increasingly high pace. This is captured well by the implemented models. The increase in damage growth rapidity is well-captured, primarily considering the steep increase in fibre failure close to final failure. This correlates with high energy signals measured close to final failure, likely due to fibre fracture.

An exception to the good correspondence is the steep increase in matrix failure and delaminations predicted by DM2 at 70 % and 80 % of the failure load - not distinctly visible in AE measurements. This can be linked to the unrealistic damage patterns observed earlier, the jump at 70 % corresponding to extensive $0°/90°$ and $90°/45°$ delamination coupled with significant matrix cracking in $90°$ and $45°$ plies, and the jump at 80 % to extensive $-45°/0°$ and $45°/-45°$ delamination coupled with significant matrix failure in $\pm 45°$ plies.

[FIGURE AE DAMAGE EVOLUTION (Figure 14) APPROXIMATELY HERE]

## 6. Conclusions and recommendations

A blended CDM and fracture mechanics methodology has been implemented in ABAQUS. A UMAT subroutine is used to model constitutive behaviour and fibre failure, XFEM through a UDMGINI subroutine to insert cohesive zones to model matrix cracking and interspersed cohesive layers to model delaminations. Validation with respect to an experimental campaign on open-hole tensile tests and comparison to a CDM based on LaRC05 damage initiation and bilinear softening, has yielded the following conclusions.

Final failure predictions by the blended methodology are in excellent cor-

respondence to the experimental failure load. Similar performance is achieved using the developed CDM.

Where the blended methodology distinguishes itself, is in its ability to capture discrete matrix cracking and the correct orientation thereof along the fibres - in line with experimental observations. The developed CDM implementation predicts excessively smeared damage and deviating failure patterns, even with cohesive zones to model delaminations. Moreover, AE observations show that the developed model is ostensibly capable of modelling the rapidity of damage growth throughout the loading process. Still, the blended methodology has a number of shortcomings related to the use of XFEM in Abaqus. Foremostly, the modelling of a single crack can underestimate the total amount of damage.

The heuristic stiffness degradation in CDMs effects a smearing of damage, altering the strain field noticeably. This alteration is disputed by DIC observations, showing little change in the strain maps. Contrary to the CDM, the blended model correctly predicts only a local change in the strain field in the vicinity of matrix cracking. The blended model is however due to the numerical implementation limited by single matrix crack per side, preventing parallel cracking.

Overall, the blended methodology is promising. Still, there is a lot of headway to be made towards high-fidelity PDA of FRPs.

Related to the blended methodology, extensive experimental campaigning and validation is recommended for different loading, geometry and material configurations. In particular, investigation of local damage features, especially delaminations, is warranted. Furthermore, the blended methodology displays numerical issues at times that warrant a more robust convergence framework in order to maximize computational efficiency and minimize the occurrence of premature analysis termination. Lastly, multiple crack modelling using XFEM is recommended, for example through the adoption of multiple enrichment regions.

## References


[1] Icardi U, Locatto S, Longo A. Assessment of Recent Theories for Predicting Failure of Composite Laminates. Applied Mechanics Reviews 2007;60(2):76. doi:10.1115/1.2515639.

[2] Kaddour AS, Hinton MJ, Soden PD, editors. Failure Criteria in Fibre Reinforced Polymer Composites: The World-Wide Failure Exercise. 1st ed.; Oxford: Elsevier Ltd; 2004. ISBN 9788578110796. doi:10.1017/CBO9781107415324.004. arXiv:arXiv:1011.1669v3.

[3] Kaddour AS, Hinton MJ. Maturity of 3D failure criteria for fibre-reinforced composites: Comparison between theories and experiments: Part B of WWFE-II. Journal of Composite Materials 2013;47(6-7):925–966. doi:10.1177/0021998313478710.

[4] Paris F. A Study of Failure Criteria of Fibrous Composite Materials. Tech. Rep.; National Aeronautics and Space Administration; Hampton, Virginia; 2001. doi:NASA/CR-2001-210661.

[5] Orifici AC, Herszberg I, Thomson RS. Review of methodologies for composite material modelling incorporating failure. Composite Structures 2008;86(1-3):194–210. doi:10.1016/j.compstruct.2008.03.007.

[6] Garnich MR, Akula VMK. Review of Degradation Models for Progressive Failure Analysis of Fiber Reinforced Polymer Composites. Applied Mechanics Reviews 2008;62(1):010801–010801–33. doi:10.1115/1.3013822.

[7] Lapczyk I, Hurtado JA. Progressive damage modeling in fiber-reinforced materials. Composites Part A: Applied Science and Manufacturing 2007;38(11):2333–2341. doi:10.1016/j.compositesa.2007.01.017.

[8] Zhang C, Li N, Wang W, Binienda WK, Fang H. Progressive damage simulation of triaxially braided composite using a 3D meso-scale finite element model. Composite Structures 2015;(125):104–116. doi:10.1016/j.compstruct.2015.01.034.

[9] van Dongen BR. Progressive damage modelling of FRPs using a blended stress-strain and fracture mechanics approach in FEM. M.sc. thesis; Delft University of Technology; 2017. URL: https://repository.tudelft.nl/islandora/object/uuid%3Ac879ec90-a2bd-42a8-884d-d66e1af2102e?collection=education.

[10] Tsai SW. Strength Characteristics of Composite Materials. Tech. Rep.; National Aeronautics and Space Administration; Washington, DC; 1965. arXiv:ADA307777.

[11] Tsai SW, Wu EM. A General Theory of Strength for Anisotropic Materials. Journal of Composite Materials 1971;5(1):58–80. doi:10.1177/002199837100500106.

[12] Hill R. A Theory of the Yielding and Plastic Flow of Anisotropic Metals. Proceedings of the Royal Society of London Series A, Mathematical and Physical Sciences 1948;193(1033):281–297.

[13] Hoffman O. The Brittle Strength of Orthotropic Materials. Journal of Composite Materials 1967;1(2):200–206. doi:10.1002/2015JB012542.

[14] Chamis CC. Failure Criteria for Filamentary Composites. In: Testing and Design, ASTM STP 460. Philadelphia: American Society for Testing and Materials; 1969, p. 336–460.

[15] Sandhu R. Nonlinear Behavior of Unidirectional and Angle Ply Laminates. Journal of Aircraft 1976;13(2):104–111.

[16] Hashin Z, Rotem A. A fatigue failure criterion for fiber-reinforced materials. Journal of Composite Materials 1973;7(4):448–464.

[17] Hashin Z. Failure Criteria for Unidirectional Fiber Composites. Journal of Applied Mechanics 1980;47(2):329–334.

[18] Puck A, Schürmann H. Failure Analysis of FRP Laminates By Means of Physically Based Phenomenological Models. Composites Science and Technology 2002;(62):1633–1662.

[19] Deuschle HM. 3D Failure Analysis of UD Fibre Reinforced Composites: Puck's theory within FEA. Phd thesis; Universität Stuttgart; 2010.

[20] Davila CG, Jaunky N, Goswami S. Failure Criteria for FRP Laminates in Plane Stress. Journal of Composite Materials 2005;39(4):323 – 345. doi:10.1177/0021998305046452.

[21] Pinho ST, Darvizeh R, Robinson P, Schuecker C, Camanho PP. Material and structural response of polymer-matrix fibre-reinforced composites. Journal of Composite Materials 2012;46(20):2313–2341. doi:10.1177/0021998312454478.

[22] Pinho ST, Dávila CG, Camanho PP, Iannucci L, Robinson P. Failure Models and Criteria for FRP Under In-Plane or Three-Dimensional Stress States Including Shear Non-linearity. Tech. Rep.; National Aeronautics and Space Administration; Hampton, Virginia; 2005. doi:NASA/TM-2005-213530.

[23] Cuntze RG. The predictive capability of failure mode concept-based strength criteria for multi-directional laminates-Part B. Composites Science and Technology 2004;64(3):976–1025. doi:10.1016/B978-008044475-8/50035-4.

[24] Cuntze RG. The predictive capability of failure mode concept-based strength conditions for laminates composed of unidirectional laminae under static triaxial stress states. Journal of Composite Materials 2012;46(19-20):2563–2594. doi:10.1177/0021998312449894.

[25] Sun CT, Quinn BJ, Tao J. Comparative Evaluation of Failure Analysis Methods for Composite Laminates. Tech. Rep.; U.S. Department of Transportation; Springfield, Virginia; 1996.

[26] Lee JD. Three dimensional finite element analysis of damage accumulation in composite laminate. Computers & Structures 1982;I(3):335–350.

[27] McCarthy CT, McCarthy MA, Lawlor VP. Progressive damage analysis of multi-bolt composite joints with variable bolt-hole clearances. Composites

Part B: Engineering 2005;36(4):290–305. doi:10.1016/j.compositesb.2004.11.003.

[28] Camanho PP, Matthews FL. A Progressive Damage Model for Mechanically Fastened Joints in Composite Laminates. Journal of Composite Materials 1999;33(24):2248–2280. doi:10.1177/07399863870092005. arXiv:0803973233.

[29] Zarouchas DS, Makris AA, Sayer F, van Hemelrijck D, van Wingerde AM. Investigations on the mechanical behavior of a wind rotor blade subcomponent. Composites Part B: Engineering 2012;43(2):647–654. doi:10.1016/j.compositesb.2011.10.009.

[30] Van der Meer FP, Sluys LJ. Continuum Models for the Analysis of Progressive Failure in Composite Laminates. Journal of Composite Materials 2009;43(20):2131–2156. doi:10.1177/0021998309343054.

[31] Van der Meer FP. Computational Modeling of Failure in Composite Laminates. Phd thesis; Delft University of Technology; 2010.

[32] Matzenmiller A, Lubliner J, Taylor RL. A constitutive model for anisotropic damage in fiber-composites. Mechanics of Materials 1995;20(2):125–152. doi:10.1016/0167-6636(94)00053-0.

[33] Maimí P, Camanho PP, Mayugo JA, Dávila CG. A continuum damage model for composite laminates: Part II - Computational implementation and validation. Mechanics of Materials 2007;39(10):909–919. doi:10.1016/j.mechmat.2007.03.006.

[34] Maimí P, Camanho PP, Mayugo JA, Dávila CG. A continuum damage model for composite laminates: Part I - Constitutive model. Mechanics of Materials 2007;39(10):897–908. doi:10.1016/j.mechmat.2007.03.005.

[35] Bažant ZP, Oh BH. Crack band theory for fracture of concrete. Matériaux et Construction 1983;16(3):155–177. doi:10.1007/BF02486267.

[36] Krueger R. Virtual crack closure technique: History, approach, and applications. Applied Mechanics Reviews 2004;57(2):109. doi:10.1115/1.1595677.

[37] Pascoe JA, Alderliesten RC, Benedictus R. Methods for the prediction of fatigue delamination growth in composites and adhesive bonds - A critical review. Engineering Fracture Mechanics 2013;112-113:72–96. doi:10.1016/j.engfracmech.2013.10.003.

[38] Elices M, Guinea G, Gómez J, Planas J. The cohesive zone model: advantages, limitations and challenges. Engineering Fracture Mechanics 2002;69(2):137–163. doi:10.1016/S0013-7944(01)00083-2.

[39] Lampani L. Finite element analysis of delamination of a composite component with the cohesive zone model technique. Engineering Computations 2011;28(1-2):30–46. doi:Doi10.1108/02644401111097000.

[40] De Morais AB. Cohesive zone beam modelling of mixed-mode I-II delamination. Composites Part A: Applied Science and Manufacturing 2014;64(September):124–131. doi:10.1016/j.compositesa.2014.05.004.

[41] Vigueras G, Sket F, Samaniego C, Wu L, Noels L, Tjahjanto D, et al. An XFEM/CZM implementation for massively parallel simulations of composites fracture. Composite Structures 2015;125(July):542–557. doi:10.1016/j.compstruct.2015.01.053.

[42] Turon A, Dávila CG, Camanho PP, Costa J. An Engineering Solution for Solving Mesh Size Effects in the Simulation of Delamination with Cohesive Zone Models. Engineering Fracture Mechanics Journal 2007;74(10):1665–1682.

[43] Jalalvand M, Czél G, Fuller JD, Wisnom MR, Canal LP, González CD, et al. Energy dissipation during delamination in composite materials - An experimental assessment of the cohesive law and the stress-strain field

ahead of a crack tip. Composites Science and Technology 2016;134:115–124. doi:10.1016/j.compscitech.2016.08.001.

[44] Camanho P, Davila C. Mixed-Mode Decohesion Finite Elements in for the Simulation Composite of Delamination Materials. Tech. Rep.; National Aeronautics and Space Administration; Hampton, Virginia; 2002. doi:10.1177/002199803034505.

[45] Harper PW, Hallett SR. Cohesive zone length in numerical simulations of composite delamination. Engineering Fracture Mechanics 2008;75(16):4774–4792. doi:10.1016/j.engfracmech.2008.06.004.

[46] Hallett SR, Green BG, Jiang WG, Wisnom MR. An experimental and numerical investigation into the damage mechanisms in notched composites. Composites Part A: Applied Science and Manufacturing 2009;40(5):613–624. doi:10.1016/j.compositesa.2009.02.021.

[47] ABAQUS. ABAQUS Documentation. Providence, RI, USA: Dassault Systèmes; 2011.

[48] Benzeggagh ML, Kenane M. Measurement of mixed-mode delamination fracture toughness of unidirectional glass/epoxy composites with mixed-mode bending apparatus. Composites Science and Technology 1996;56(4):439–449. doi:10.1016/0266-3538(96)00005-X.

[49] Fries T, Belytschko T. The extended/generalized finite element method: An overview of the method and its applications. International Journal for Numerical Methods in Engineering 2010;84(3):253–304. doi:10.1002/nme.arXiv:1201.4903.

[50] Puck A, Schürmann H. Failure analysis of FRP laminates by means of physically based phenomenological models. Composites Science and Technology 1998;(58):1045–1067. doi:10.1016/B978-008044475-8/50028-7.

[51] Nixon-Pearson OJ, Hallett SR. An investigation into the damage development and residual strengths of open-hole specimens in fatigue. Composites

Part A: Applied Science and Manufacturing 2015;69:266–278. doi:10.1016/j.compositesa.2014.11.013.

[52] Nixon-Pearson OJ, Hallett SR, Harper PW, Kawashita LF. Damage development in open-hole composite specimens in fatigue. Part 2: Numerical modelling. Composite Structures 2013;106:890–898. doi:10.1016/j.compstruct.2013.05.019.

[53] Czabaj M, Ratcliffe J. Comparison of intralaminar and interlaminar mode-I fracture toughness of unidirectional IM7/8552 graphite/epoxy composite. Composites Science and Technology 2013;89(December):15–23.

[54] Walker TH, Avery WB, Ilcewicz LB, Poe, C C J, Harris CE. Tension fracture of laminates for transport fuselage. Part 1: Material screening. In: Ninth DOD(NASA)FAA Conference on Fibrous Composites in Structural Design. 1992, p. 747–787.

[55] Hexcel 8552. Epoxy Matrix Product Datasheet. Online; Accessed: 01-02-2017. URL: http://www.hexcel.com/user_area/content_media/raw/HexPly_8552_eu_DataSheet.pdf.

[56] Zarouchas DS, Antoniou AE, Sayer F, Van Hemelrijck D, van Wingerde AM. Structural Integrity Assessment of blade's subcomponents using Acoustic Emission Monitoring. In: Proulx T, editor. Experimental and Applied Mechanics, Volume 6: Proceedings of the 2011 Annual Conference on Experimental and Applied Mechanics. New York, NY: Springer New York. ISBN 978-1-4614-0222-0; 2011, p. 511–518. doi:10.1007/978-1-4614-0222-0_61.

[57] Camanho PP, Dávila CG, Pinho ST, Iannucci L, Robinson P. Prediction of in situ strengths and matrix cracking in composites under transverse tension and in-plane shear. Composites Part A: Applied Science and Manufacturing 2006;37(2):165–176. doi:10.1016/j.compositesa.2005.04.023.

[58] Parvizi A, Garrett KW, Bailey JE. Constrained cracking in glass fibre-reinforced epoxy cross-ply laminates. Journal of Materials Science 1978;13(1):195–201. doi:10.1007/BF00739291.

[59] Ersoy N, Garstka T, Potter K, Wisnom MR, Porter D, Clegg M, et al. Development of the properties of a carbon fibre reinforced thermosetting composite through cure. Composites Part A: Applied Science and Manufacturing 2010;41(3):401–409. doi:10.1016/j.compositesa.2009.11.007.

[60] Perogamvros NG, Lampeas GN. Experimental and numerical investigation of AS4/8552 interlaminar shear strength under impact loading conditions. Journal of Composite Materials 2016;50(19):2669–2685. doi:10.1177/0021998315610899.

[61] Badalló P. Analysis and Optimization of Composite Stringers. Ph.D. thesis; Universitat de Girona; 2015.

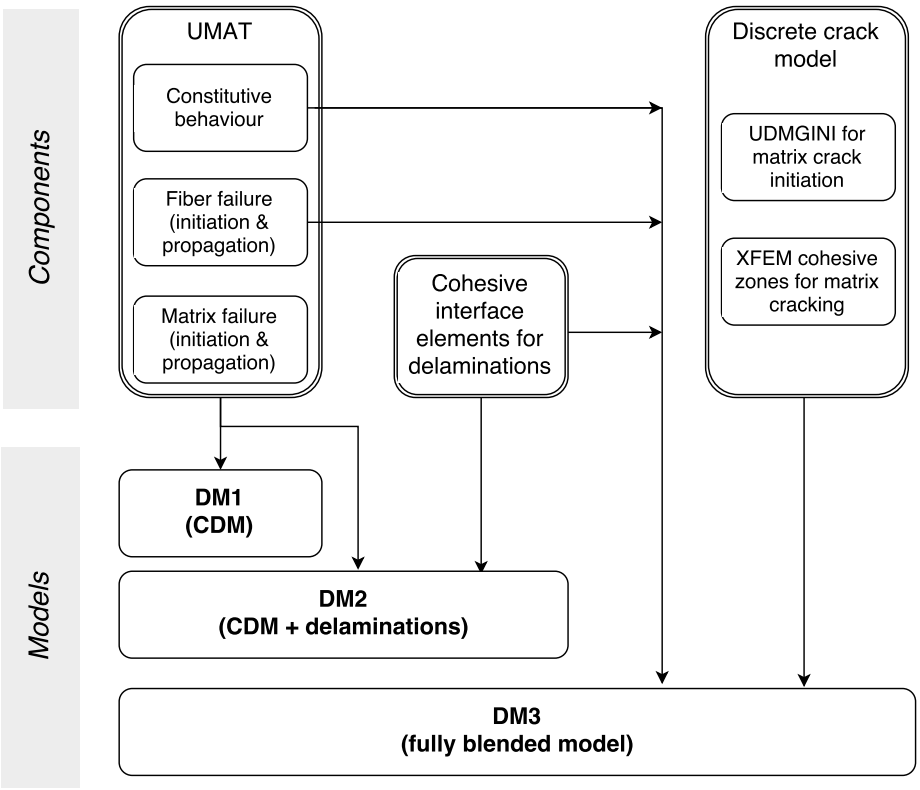


Figure 1: Schematic overview of blended model synthesis

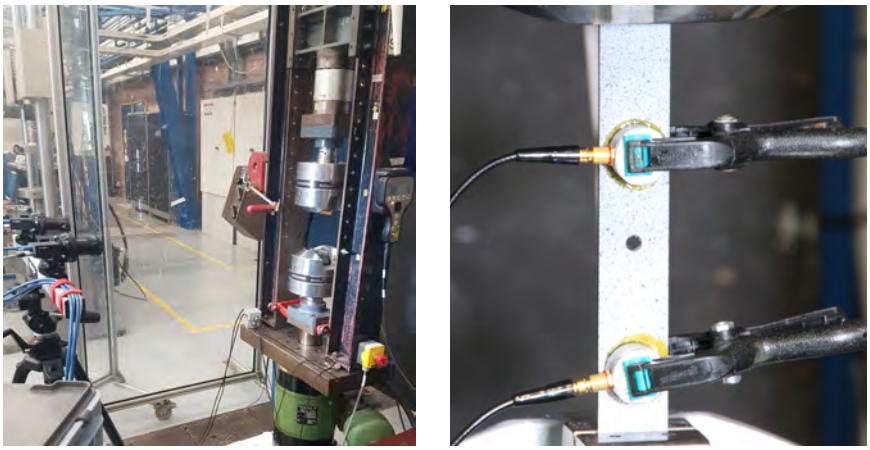

(a) DIC and test set-up (b) Specimen and AE sensor placement

Figure 2: Experimental set-up

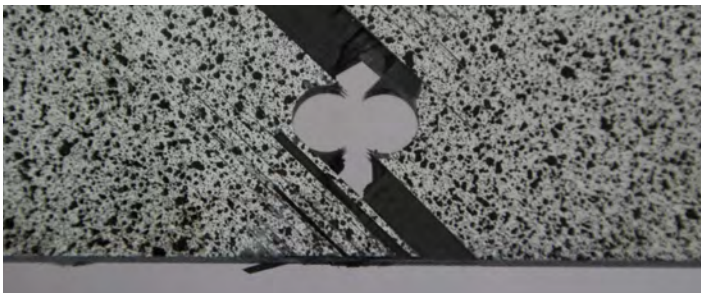

(a) Top view

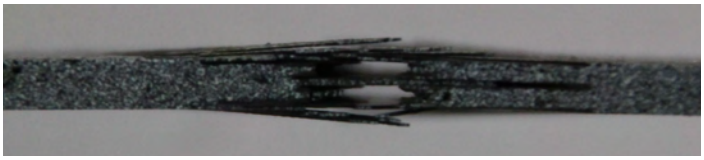

(b) Side view

Figure 3: Specimen failure pattern after ultimate (pull-out) failure. Loading direction: horizontal in page

(a) Outer $-45°$ ply (b) Outer $0°$ ply (c) Outer $90°$ ply

Figure 4: X-ray CT scans of observed damage after ultimate (pull-out) failure. Loading direction: horizontal in page

Table 1: Experimental results for final failure

| Specimen | Failure load [kN] | Failure stress [MPa] | CV [%] |
|---|---|---|---|
| 1 | 26.06 | 386.1 | |
| 2 | 26.30 | 389.6 | |
| 3 | 27.27 | 404.0 | |
| 4 | 27.32 | 404.7 | |
| 5 | 27.04 | 400.6 | |
| 6 | 25.44 | 376.9 | |
| Average | 26.2 | 388.2 | 3.1 |

Table 2: Predicted and measured final failure stress for experimental case

| Model | Predicted [MPa] | Discrepancy | |
|---|---|---|---|
| | | [MPa] | [%] |
| DM1 | 399.8 | 14.8 | 3.9 |
| DM2 | 355.6 | -29.4 | -7.6 |
| DM3 | 394.1 | 9.1 | 2.4 |

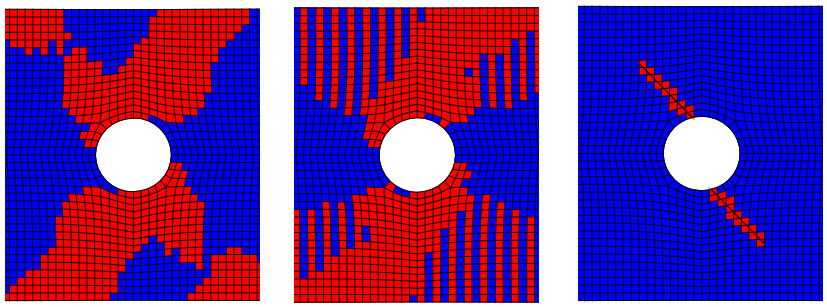

(a) DM1 (b) DM2 (c) DM3

Figure 5: Progression of matrix failure in outer $-45°$ ply for experimental test case at 90% of failure load (red and blue denote respectively damaged and undamaged elements). Loading direction: horizontal in page

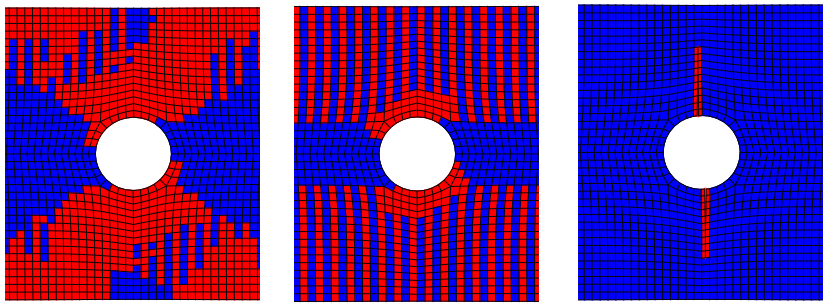

(a) DM1 (b) DM2 (c) DM3

Figure 6: Progression of matrix failure in outer 90° ply for experimental test case at 90% of failure load (red and blue denote respectively damaged and undamaged elements) Loading direction: horizontal in page

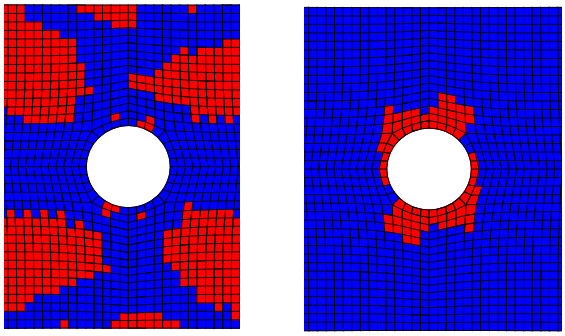

(a) DM2 (b) DM3

Figure 7: Progression of delamination in outer $45°/-45°$ interface for experimental test case at 90% of failure load (red and blue denote respectively damaged and undamaged elements). Loading direction: horizontal in page

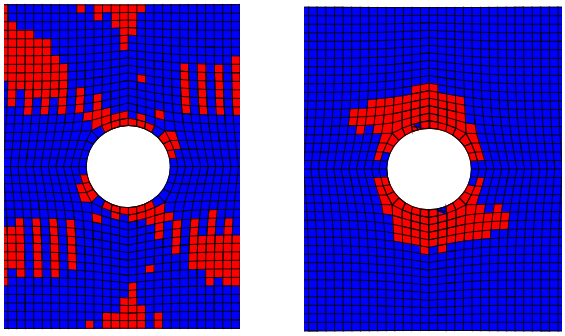

(a) DM2 (b) DM3

Figure 8: Progression of delamination in outer $-45°/0°$ interface for experimental test case at 90% of failure load (red and blue denote respectively damaged and undamaged elements). Loading direction: horizontal in page

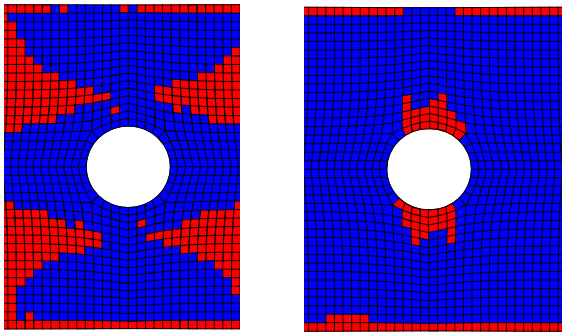

(a) DM2 (b) DM3

Figure 9: Progression of delamination in outer $0°/90°$ interface for experimental test case at 90% of failure load (red and blue denote respectively damaged and undamaged elements). Loading direction: horizontal in page

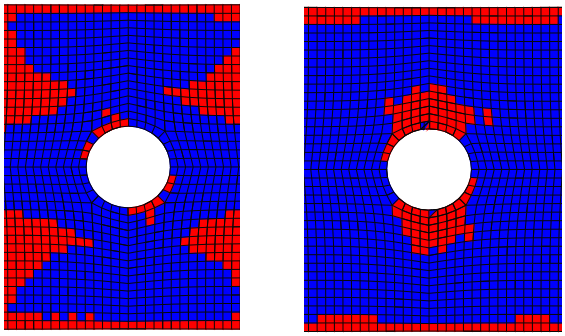

(a) DM2 (b) DM3

Figure 10: Progression of delamination in outer 90°/45° interface for experimental test case at 90% of failure load (red and blue denote respectively damaged and undamaged elements). Loading direction: horizontal in page

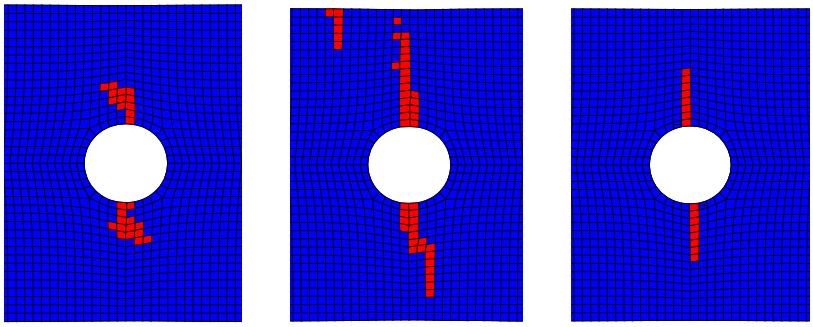

(a) DM1 (b) DM2 (c) DM3

Figure 11: Progression of fibre failure in outer 0° ply for experimental test case at final failure (red and blue denote respectively damaged and undamaged elements). Loading direction: horizontal in page

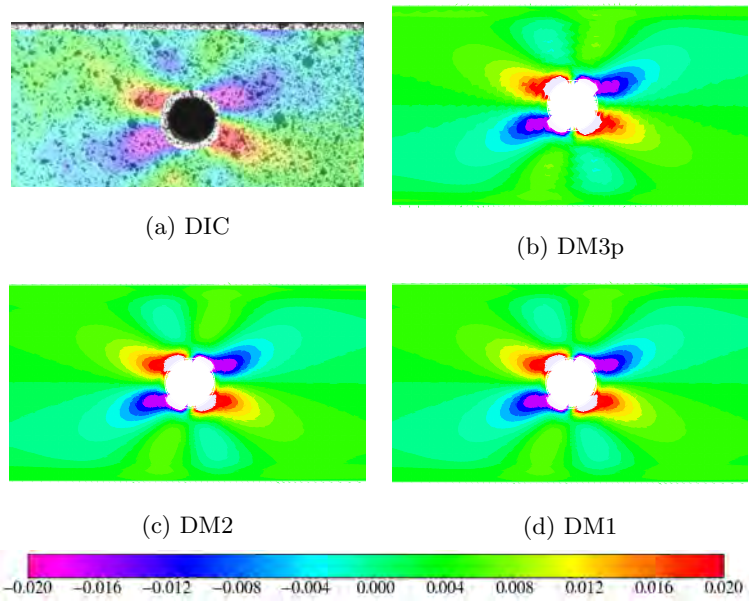


Figure 12: Comparison of measured and predicted strain field at 10 % of failure load (white areas denote strain outside of spectrum)

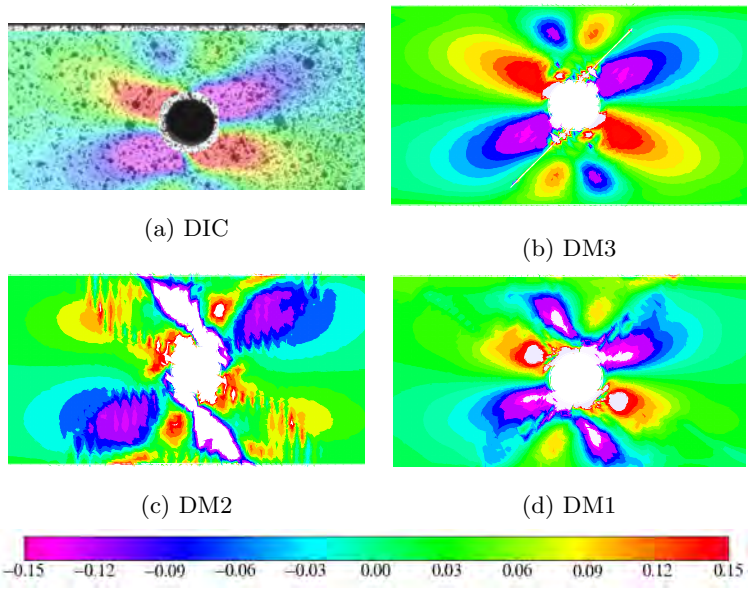


Figure 13: Comparison of measured and predicted strain field at 95 % of failure load (white areas denote strain outside of spectrum)

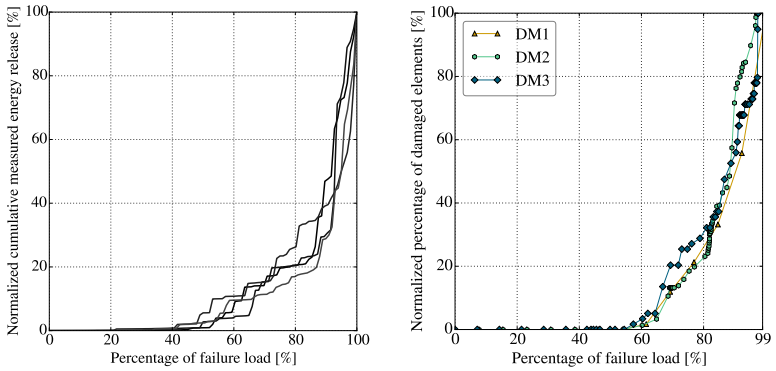


(a) AE

(b) fibre failure

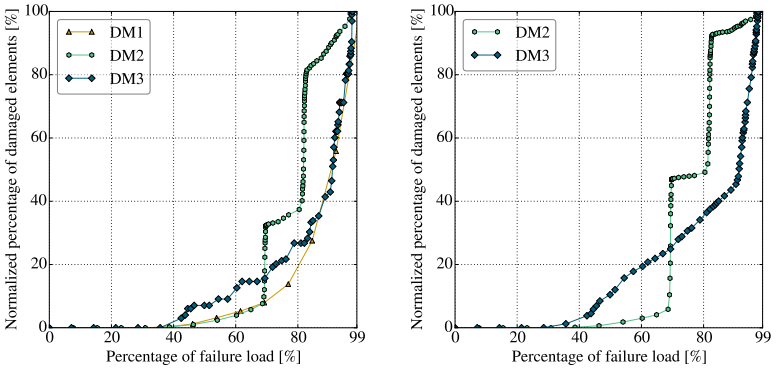


(c) Matrix failure

(d) Delamination

Figure 14: Predicted damage evolution experimental test case

Table 3: Material properties for AS4/8552

| **General [60, 59, 61]** | |
|---|---|
| $E_1$ [GPa] | 135 |
| $E_2$ [GPa] | 9.5 |
| $\nu_{12}$ [-] | 0.32 |
| $\nu_{23}$ [-] | 0.45 |
| $G_{12}$ [GPa] | 4.9 |
| $G_{23}$ [GPa] | 3.2 |
| $X_T$ [MPa] | 2207 |
| $X_C$ [MPa] | 1531 |
| $Y_T$ (thin embedded ply) [MPa] | 145 |
| $Y_T$ (thick embedded ply) [MPa] | 82 |
| $Y_T$ (outer ply) [MPa] | 96 |
| $Y_C$ [MPa] | 200 |
| $S_{12}$ (thin embedded ply) [MPa] | 133 |
| $S_{12}$ (thick embedded ply) [MPa] | 111 |
| $S_{12}$ (outer ply) [MPa] | 111 |
| $\alpha_0$ [deg] | 53 |
| **Bilinear softening [60, 59]** | |
| $G_{fft}$ [N/mm] | 92.0 |
| $G_{ffc}$ [N/mm] | 80.0 |
| $G_{mft}$ [N/mm] | 0.30 |
| $G_{mfc}$ [N/mm] | 0.80 |
| **Puck [19]** | |
| $p^c_{\perp\perp}$ [-] | 0.325 |
| $p^t_{\perp\perp}$ [-] | 0.325 |
| $p^c_{\perp\parallel}$ [-] | 0.35 |
| $p^t_{\perp\parallel}$ [-] | 0.30 |
| **Cohesive zones [60]** | |
| $\sigma_I^{max}$ [MPa] | 80.7 |
| $\sigma_{II}^{max}$ [MPa] | 114.5 |
| $G_{Ic}$ [N/mm] | 0.3 |
| $G_{IIc}$ [N/mm] | 1.0 |
| $\eta_{BK}$ [-] | 2.08 |